Thermal structural disorder and melting at a crystalline interface

Tue Nguyen*
Department of Nuclear Engineering, Massachusetts Institute of Technology, Cambridge, Massachusetts 02139 and IBM Burlington, Essex Junction, Vermont 05452

Paul S. Ho† and Thomas Kwok
IBM Thomas J. Watson Research Center, Yorktown Heights, New York 10598

Cynthia Nitta
Lawrence Livermore Laboratory, Livermore, California 94550

Sidney Yip
Department of Nuclear Engineering, Massachusetts Institute of Technology, Cambridge, Massachusetts 02139
(Received 12 December 1991)

Thermal disordering and melting at a grain boundary are investigated by molecular dynamics in an internally consistent simulation model that avoids a number of pitfalls of earlier models. The bulk melting temperature T_m of the model system, specified by an embedded-atom-method potential function fitted to aluminum, is first determined by observing directly surface-nucleated melting in a single-crystal cell with free surfaces. Simulation is then carried out on a bicrystal cell with a high-angle symmetrical tilt grain boundary on the $(\bar{1}30)$ plane. Profiles across the interface of local structural order and energy, along with data on atomic mobility, are obtained at several temperatures from below T_m to above T_m; the results indicate that melting is nucleated at the grain boundary in a similar manner as at the free surface, and that there is no evidence of premelting. In the surface region as well as the grain-boundary core, thermal disordering at temperatures below T_m was observed with characteristic metastable behavior commencing at about 0.93 T_m. The temperature variation of the interfacial thickness suggests that the onset of disordering is a continuous process.

I. INTRODUCTION

In the study of physical properties of grain-boundary materials at elevated temperatures,[1] the structural stability of a bicrystalline interface in the presence of atomic disordering is of fundamental concern. Because the interfacial region is typically of atomic dimensions, direct observations of structural integrity are extremely difficult. As a result, one has turned to molecular-dynamics simulations to investigate the atomic structure at the interface over a temperature range up to the melting point of the crystal.[2–5] All the simulation studies found that thermal disordering sets in at a fairly low temperature (typically, initial structural distortions were observed at $T=0.5T_m$, where T_m is the melting point of the bulk material). However, different simulations have given essentially conflicting results concerning the nature of disordering in the interfacial region.[2–5] In particular, there was disagreement concerning the possible occurrence of premelting in high-angle tilt boundaries. Premelting is defined here to mean the complete loss of crystalline order at the interface at a temperature distinctly below T_m. In interpreting the various simulation results it is necessary to bear in mind that the different models and simulation procedures employed could lead to artifacts. This situation was reviewed by Pontikis, who pointed out a number of possible reasons for the conflicting conclusions.[6]

On the experimental side, a number of grain-boundary measurements exist which suggest some kind of structural transition could be taking place at temperatures well below T_m.[7,8] However, none of these data could be regarded as direct evidence of grain-boundary premelting. Recently, TEM studies based on the imaging of grain-boundary dislocations have shown that in a bicrystal specimen of aluminum, premelting was not observed up to essentially T_m.[9] Despite this important finding, we are still lacking detailed information on the atomic-level behavior of the interface structure at elevated temperatures.

In this paper we present a molecular-dynamics study of atomic disordering at a free surface and at a grain boundary over a range of temperatures including the melting point T_m.[10] Using a simulation model consisting of a single crystal with free surfaces, we have observed local melting nucleated at the surfaces. By determining the propagation velocity of the melt-crystal interface at several temperatures and extrapolating to zero velocity,[11,12] we determined T_m for the simulation model. Repeating this study using a simulation consisting of a bicrystal with free surfaces, we found that melting was also nucleated at the crystalline interface, and from the associated propagation velocities, the same melting temperature was obtained. Our results show that, while significant structural disordering occurs at $T<T_m$, there is no evidence pointing to premelting at the grain boundary. This finding is different from our own previous inter-

pretations,[3] but is in agreement with the conclusion of Ciccotti, Guillope, and Pontikis,[2] who studied the same grain boundary using periodic border conditions, as well as that of Phillpot *et al.*[11] and Lutsko *et al.*[12] in more recent studies of a different boundary using a border condition developed specifically for interface systems.[13]

In the present work we have studied the nature of surface and grain-boundary disordering at temperatures below T_m. We found that the local structure, potential energy, and atomic mobility of the disordered region can be quite liquidlike, but such behavior is found to be metastable, and over a long interval of simulation the underlying crystalline order can re-emerge. There appears to be close similarity between the properties of the disordered region at a free surface and that at a grain boundary; in both cases the onset of disordering seems to be a continuous process.

In Sec. II we describe our bicrystal model, the interatomic potential function to be used, and the various properties to be analyzed. In Sec. III we examine the simulation results of heating a single-crystal cell with periodic border conditions (cell A) to various temperatures; the data constitute the reference bulk properties for the crystalline and liquid states. In Sec. IV we present the simulation results obtained using a single-crystal cell with free surfaces along one direction (cell B). These data allow us to determine the melting point of our model T_m, as well as to study surface disordering above and below T_m. In Sec. V the simulation results of a bicrystal cell with free surfaces (cell C) are discussed, showing that local melting nucleated at the grain boundary leads to the same value of T_m, and that disordering in the grain-boundary region is similar to that at the free surface. Sec. VI presents a summary and concluding remarks.

II. SIMULATION MODELS AND PROCEDURES

A. Bicrystal cell geometry and border conditions

In this work we will study three simulation models: cell A representing a single bulk crystal; cell B representing a single crystal with two parallel free surfaces; and cell C representing a bicrystal also with free surfaces. All three systems are fcc lattices with crystal orientations depicted in Fig. 1. The bicrystal cell used to model a high-angle grain boundary is oriented with the interface lying on the $(\bar{1}30)$ plane. Its structure is that of a symmetrical tilt grain boundary, conventionally specified by a tilt or misorientation angle of 36.86° about an axis along $\langle 001 \rangle$ ($\Sigma=5$). From the standpoint of specifying the appropriate degrees of freedom of the particular solid interface, it is actually more useful to recognize this structure as a special case of symmetrical twist grain boundaries with $(\bar{1}30)$ as the interfacial plane, the twist angle being 180°.[14]

For border conditions on the simulation cell, all systems are taken to be periodic along the x and y directions ($\{310\}$ and $\{001\}$, respectively). Along the z direction ($\{\bar{1}30\}$), cell A also has periodic borders, whereas cells B and C have free border conditions. Cell A is a cube with three unit cells along each side, containing 108 atoms. Cells B and C are identical in dimensions, which are 2

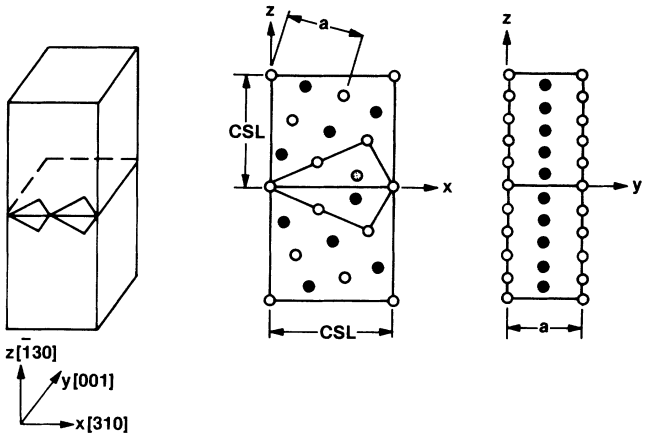

FIG. 1. Bicrystal simulation cell showing the crystallographic orientation of a symmetrical tilt boundary on the $(\bar{1}30)$ plane. Also shown are the x-z and y-z plane projections of two adjacent layers of atoms (open and closed circles) in 2 CSL structural units along the z direction [1 CSL$=(\sqrt{2.5})a$, where a is the lattice constant]. The shaded atom will be removed before starting the simulation.

CSL, $3a$, and 32 CSL, respectively, in the x, y, and z directions, where a CSL unit is $(\sqrt{2.5})a$, and a is the lattice constant (see Fig. 1). Each cell is a stack of 320 $(\bar{1}30)$ planes with 6 atoms per plane for a total of 1920 atoms in the system. Choosing a relatively small interfacial plane for study minimizes possible complications due to curvature effects. The z dimension is taken to be as large as our computational resources allow in order to provide maximum separation between the interface and the free surfaces.

The atomic structure of our bicrystal model is created by taking a fcc crystal, cutting it in half along a (310) plane, rotating one half with respect to the other by 180°, and putting the two half crystals back together. In this configuration there will be a pair of atoms in very close proximity to each other in each of the two CSL units across the boundary (see Fig. 1). To avoid this unphysical, high-energy local configuration, it is conventional to remove one of the atoms and allow the entire system to relax.[15] With the present free-surface border conditions, relaxation can occur in all three directions, relative translations of the two halves of the bicrystal as well as local expansion or contraction in the z direction in the interfacial region.

B. Interatomic potentials

The interatomic interaction potential function adopted for the present study is constructed by means of the embedded-atom method (EAM).[16] The potential has been fitted to the known properties of pure aluminum, namely, elastic constants, sublimation energy, lattice constant, and vacancy formation energy. In this approach the total energy of the system is written as

$$E_{\rm tot}=\sum_i F_i\left[\sum_{j(\neq i)}\rho_j(r_{ij})\right]+\frac{1}{2}\sum_{\substack{i,j\\(i\neq j)}}\phi_{ij}(r_{ij})\ , \qquad (1)$$

where $\rho_j(r_{ij})$ is the electron density contributed by atom j at atom i, and ϕ_{ij} is the short-range pair interaction between atoms i and j.

In our case ϕ_{ij} is taken to be a Morse potential

$$\phi(r)=D_0\{\exp[-2\alpha(r-r_0)]-2\exp[-\alpha(r-r_0)]\}\ , \quad (2)$$

with $D_0=0.259\,59$ eV, $\alpha=2.658\,03$ Å^{-1}, and $r_0=1.880\,67$ Å.

For the electron density we use only the longest-range parts of results of Hartree-Fock calculations,[17] and for the embedding function F_i we use a simplified universal equation of state.[18] Both the pair potential ϕ and the density ρ are cut off at 5.45 Å, which is between fourth- and fifth-nearest neighbors, and a constant is added to each so they approach zero continuously at the cutoff.

C. Property calculations

We will examine those physical properties that are well defined at any temperature and that reveal some aspects of structural order. The properties to be calculated are the potential energy U, the radial distribution function $g(r)$, the static structure $S(K)$, and the mean-square displacement $\Delta r^2(t)$. They are defined as follows:

$$U=E_{\rm tot},\quad i,j\in L\ , \quad (3)$$

$$\rho g(r)=\left\langle \sum_{i,j\in L}\delta(r-r_{ij},\Delta r)/V(r_i,r,\Delta r)\right\rangle /N\ , \quad (4)$$

$$S(K)=\left|\sum_{i\in L}\exp(iK\langle r_i\rangle)\right|^2/N^2\ , \quad (5)$$

$$\Delta r^2(t)=\left\langle \sum_{i\in L}[r_i(t)-r_i(0)-r_{\rm c.m.}(t)+r_{\rm c.m.}(0)]^2\right\rangle\ . \quad (6)$$

Since we are interested in how these properties vary with distance from the interface, we will divide the simulation cell into equal layers and carry out the property calculations for each individual layer. In these expressions, L specifies the particular layer, u is the interatomic pair potential, r_i is the position of atom i, $r_{ij}=|\mathbf{r}_i-\mathbf{r}_j|$, ρ is the bulk density, $V(r_i,r,\Delta r)$ is the volume of a spherical shell centered at r_i with radius r and thickness Δr, K is a prescribed wave vector chosen in this work to be along the y direction, N is the number of atoms in layer L, $r_{\rm c.m.}$ is the center-of-mass position of layer L. The ensemble average, denoted by the angular bracket $\langle\ \rangle$, will be treated as a time average over the simulated trajectories, and δ is a modified delta function defined as

$$\delta(r,\Delta r)=\begin{cases}1 & \text{if } -\Delta r/2\le r\le \Delta r/2\\ 0 & \text{otherwise}\ .\end{cases} \quad (7)$$

Our expression for the static structure factor differs somewhat from the conventional definition in that the particle position r_i is replaced by the average position $\langle r_i\rangle$. We find that by using the time-averaged position, the smearing effect of thermal vibrations is greatly reduced.

In analyzing our results, we divide the simulation cell into 64 equal slices along the z direction, each having a width of $\frac{1}{2}$ CSL ($0.79a$) and containing 30 atoms at the outset. The above properties will be examined both in terms of their values for the entire cell and their layer profiles. The size of a layer is chosen to be small enough to give some spatial resolution, yet still large enough to have meaningful statistics.

III. THERMAL DISORDERING IN BULK CRYSTALS

We first consider simulations using cell A to establish the properties of our reference bulk crystal. Results of the simulations, carried out at constant temperature and constant volume with a temperature-dependent lattice constant, covering a temperature range 400–1400 K, are summarized in Table I.[10] The series starts at a low temperature, with the atomic configuration at the end of the run taken to be the initial configuration at the next temperature. The runs are made in 20 000 time steps except those at 900 and 950 K, which have been extended out to 80 000 steps.

The potential-energy results in Table I show a linear variation with temperature up to 950 K. The value at room temperature, −3.55 eV, is close to the experimental value of the cohesive energy, −3.58 eV. At 1000 K the energy increases to a distinctly higher value almost instantaneously. In examining the longer runs at 900 and 950 K, we find that in the former the energy remains reasonably constant throughout the 80 000 time steps, whereas in the latter an abrupt increase in energy takes place at 50 000 time steps. At 950 K, corresponding to the energy increase, the system configuration becomes structurally disordered as indicated by the static structure factor $S(K)$; also the mean-squared displacement increases sharply and appears to be unbounded. We regard this collection of properties as indicating a lattice instability which sets in at 950 K for the present model.[11,12]

Recent simulation studies of interface-nucleated melting show that in the absence of an interface, a single crys-

TABLE I. Summary of simulation runs using a single-crystal model with periodic border conditions (Cell A) (Ref. 10). Results shown are temperatures T (K), lattice constant a (Å), pressure P (eV/a_0^3), potential energy per atom U (eV), static structure factor $S(K)$, and mean-squared displacement MSD (a^2). a_0 is the room-temperature lattice constant (4.05 Å).

T	a	P	U	$S(K)$	MSD
400	4.094	−0.0005	−3.525	0.998	0.003
600	4.121	0.0008	−3.493	0.997	0.005
700	4.136	−0.0011	−3.476	0.998	0.006
800	4.152	0.0019	−3.457	0.996	0.008
900	4.172	0.0007	−3.436	0.995	0.013
950	4.181	0.0010	−3.418	0.993	0.013[a]
975	4.257	0.0010	−3.345	0.005	1.05[a]
1000	4.270	−0.0008	−3.335	0.010	2.89[a]
1100	4.293	−0.0039	−3.315	0.011	8.93[a]
1200	4.320	−0.0012	−3.290	0.010	18.9[a]
1300	4.339	−0.0001	−3.273	0.010	26.4[a]
1400	4.370	−0.0027	−3.248	0.009	37.7[a]

[a]MSD values at the end of the simulation run, with MSD increasing steadily with time.

tal can be superheated to a temperature where the lattice becomes unstable against shear deformation.[11,12] This process of disordering is homogeneous in nature and may be called mechanical melting. We believe the instability that sets in at 950 K in the present simulation is the manifestation of mechanical melting. This means that prior to the onset of the instability, the system is in a superheated state. However, the precise extent of the superheating is not known until one determines the value of T_m. Ignoring the distinction between thermodynamic and mechanical melting for the moment and regarding the potential-energy results as indication of a solid branch and a liquid branch, an estimate of the heat of fusion as 9.2 kJ/mol can be calculated to compare against the experimental value of 10.79 kJ/mol.

IV. THERMAL DISORDER IN A MODEL WITH FREE SURFACES

Recent simulations investigating the role of an interface in the initiation of melting have shown that, in the presence of a free surface, melting occurs as a heterogeneous process of nucleation and growth at the surface.[11,12] A different question is the nature of surface-induced disordering at temperatures below T_m. This process is also of current interest because of experimental evidence showing the existence of liquidlike surface layers well below T_m,[19] and theoretical analysis suggesting that surface properties can behave in a more continuous manner than those of the bulk.[20]

In this section we study the atomic disordering on free surfaces using simulation cell B. Our intention is to examine structural and kinetics behavior not only in anticipation of the bicrystal study using cell C, but also because such simulation results are of intrinsic interest by themselves. Another motivation is the determination of the thermodynamic melting temperature T_m for our simulation model, which is necessary for the interpretation of possible grain-boundary premelting effects.

A. Results

We have carried out simulations using cell B over a temperature range up to 950 K, the instability point observed in our model of the bulk crystal (cell A). For starting atomic configurations we again used the final configuration of the preceding run if the surfaces were still well ordered. Otherwise, a configuration at a lower temperature where the surfaces did not disorder was used.

Table II shows the potential-energy and pressure data obtained at each temperature.[10] One can infer from the pressure results that there was no significant thermal stress induced due to the temperature variation, or, equivalently, the value of the lattice constant chosen at each temperature was about correct. For the potential energy we give results separately for the ordered and the disordered regions. The distinction is primarily on the basis of the static structure factor $S(K)$, with K chosen along (001). Figure 2 shows the layer profiles of the potential energy and static structure factor obtained at 875

TABLE II. Summary of simulation runs using a single-crystal model with free surfaces (Cell B) (Ref. 10). Results shown are temperature T (K), number of time steps N_t, duration of simulation $N_t\Delta t$ (ps), pressure P (eV/a_0^3), potential energy per atom (eV/atom) in ordered and disordered layers, U_{ord} and U_{dis}, respectively. a_0 is the room-temperature lattice constant (4.05 Å), and eV/a_0^3 is equivalent to 24.1 kbar.

T	N_t	$N_t\Delta t$	P	U_{ord}	U_{dis}
400	5 000	10.42	−0.020(20)	−3.525(2)	
500	5 000	10.45	−0.022(20)	−3.510(5)	
600	5 000	10.49	−0.024(20)	−3.493(7)	
700	5 000	10.53	−0.015(20)	−3.476(7)	
750	5 000	10.55	−0.022(40)	−3.467(11)	
800	67 000	141.6	−0.021(30)	−3.457(12)	−3.385(15)[a]
825	120 000	253.9	−0.023(20)	−3.452(12)	−3.380(15)[a]
850	168 000	355.9	−0.022(30)	−3.448(12)	−3.370(15)[a]
875	147 000	311.8	−0.025(30)	−3.440(15)[b]	−3.365(15)[c]
900	16 000	33.97	−0.020(20)	−3.438(15)[b]	−3.357(15)[c]
925	15 000	31.89	−0.021(30)	−3.425(15)[b]	−3.351(15)[c]

[a]The disordered layers are observed to be metastable (see text).
[b]The ordered layers are observed to be unstable.
[c]The disordered region is observed to be expanding during simulation.

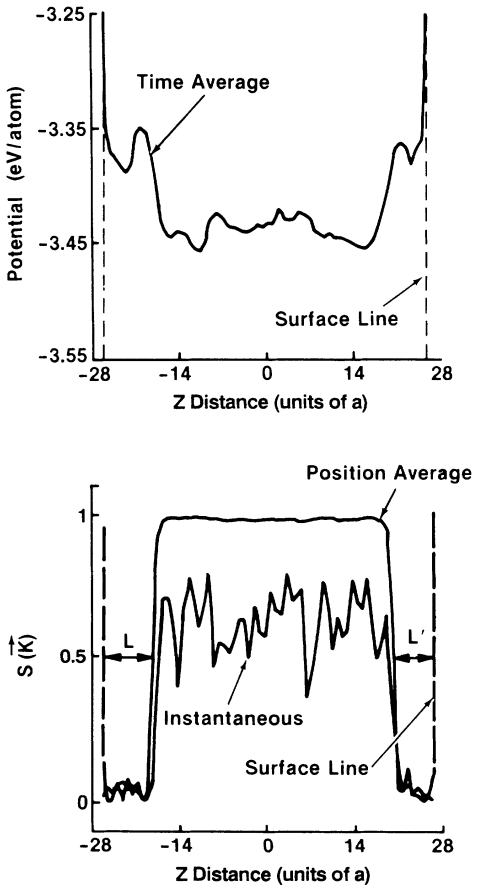

FIG. 2. Layer profiles of (a) potential energy and (b) static structure factor showing the existence of two disordered (free-surface) regions with correspondingly higher energy in cell B at 875 K. Data are averaged over 1000 time steps (2.1 ps) starting at time step 30 000.

K by averaging the data over 1000 steps starting at time step 30 000. One can observe two distinct regions besides the surface layers: a low-energy region that is well ordered, and a high-energy region that is disordered. The ordered region is always in the middle of the cell, as one would expect, and its energies are similar to those obtained from cell A (recall Table I). The disordered regions are near the surfaces; their energies are higher than those of the bulk but still significantly lower than that of the first layer of the free surface.

Table II shows that for temperatures 750 K and below no disordered region ($S \leq 0.2$) was observed during the indicated intervals of simulation. From 800 to 850 K, the surface layers became disordered intermittently, a behavior which we interpret as characteristic of metastability. Since the disordered regions persisted long enough (several picoseconds or more) to allow an estimate of time-averaged potential energy, the values so obtained are given in the table. At 875 K and beyond, the disordered regions initially formed at the surfaces were observed to expand toward the cell interior in a fairly steady fashion. However, it was still possible to distinguish between ordered and disordered regions and obtain estimates of time-averaged potential energies in each.

Figure 3 shows the temperature variation of the potential energies obtained using cells A and B. The energies are seen to form two branches: a solid branch consisting of values obtained from cell A before the onset of mechanical melting and values from cell B considering only the ordered regions; and a liquid branch made up of values from cell A after mechanical melting and values from cell B considering only the disordered regions. On the solid branch, the energy values from the two cells are very close, confirming that the ordered region in cell B is indeed bulk material. As for the liquid branch, the temperature ranges studied for the two cells do not overlap since we have purposely chosen to study cell B at temperatures below T_s (950 K). Still, the data from cell B connect smoothly onto the data from cell A. Figure 3 shows clearly a hysteresis or van der Waals loop in the 800–950 K region which is characteristic of metastability in the presence of a first-order phase transition. In simulation studies such loops are typically associated with melting transitions.[21]

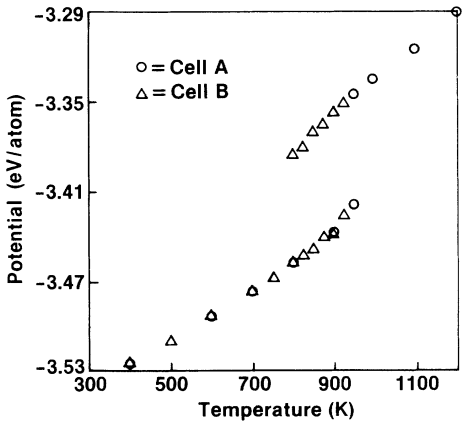

FIG. 3. Variation of potential energy per atom with temperature. Data from single crystal with periodic border conditions (cell A) and single crystal with free surfaces (cell B) are denoted by open circles and triangles, respectively.

B. Determination of T_m

We now take up the question of determining the thermodynamic melting point of our simulation model. Since T_m is the temperature at which the free energies of the solid and liquid phases are equal, a direct determination of T_m can be made by calculation of (using molecular dynamics (MD)] the Gibbs free energies. Recently this procedure has been applied to obtain T_m in two cases: a model of silicon[22] based on an empirical potential function with three-body interactions;[21] and a model of copper[12] based on an EAM potential.[16] For both potential models, an alternative method of locating T_m which avoids the free-energy calculation has also been applied and shown to give essentially the same results.[11,12] In this study we will follow the latter method.

The basis of the method we use assumes that if one can determine the temperature variation of the propagation velocity of the melt-crystal interface in a crystal under superheated condition, then the temperature at which this velocity vanishes is the temperature at which the melt and crystal phases coexist, or T_m by definition.

To apply this method we need to be able to identify the melt-crystal interface and follow its evolution during the simulation. Since the static structure factor $S(K)$ evaluated for a layer has a value close to unity when the region is well ordered, and close to zero when it is disordered, we adopt the somewhat arbitrary value of $S(K)=0.5$ as the criterion for locating the melt-crystal interface. Using this procedure we find the temporal variation of the thickness of the disordered region at several temperatures as shown in Fig. 4. At 850 K, thermal disordering effects appear to be confined to only a few surface layers in extent. While the disordered regions form and disappear, there is apparently no spreading of disordering over a long interval of simulation (over 300 ps). In contrast, the behavior at 875 K shows a persistent increase of the disordered region. At still higher temperatures one finds

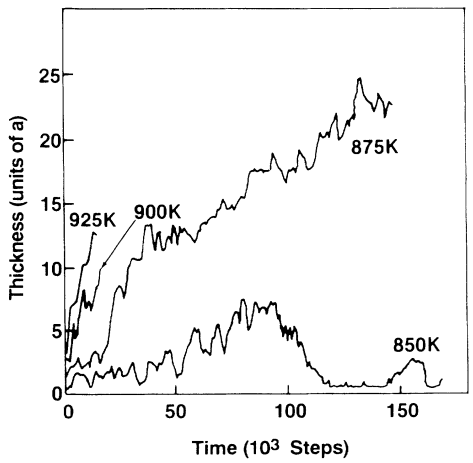

FIG. 4. Time variation of the surface-disordered region in cell B. The time unit is 1000 steps or 2.1 ps.

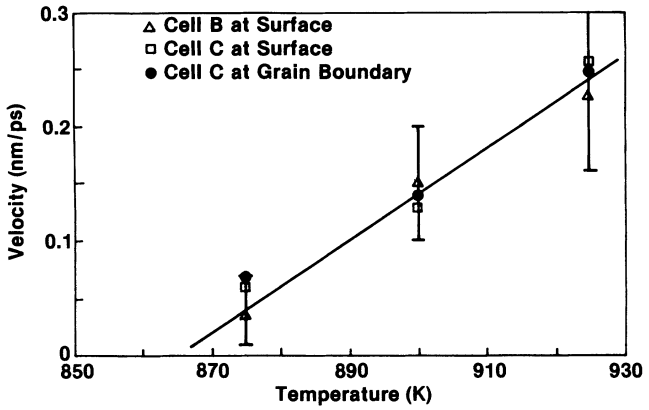

FIG. 5. Variation of propagation velocity (nm/ps) of the disordered region with temperature as determined from simulation results for cells B (open triangles) and C (open squares for surface and closed circles for grain boundary). The solid line is a linear fit through the data.

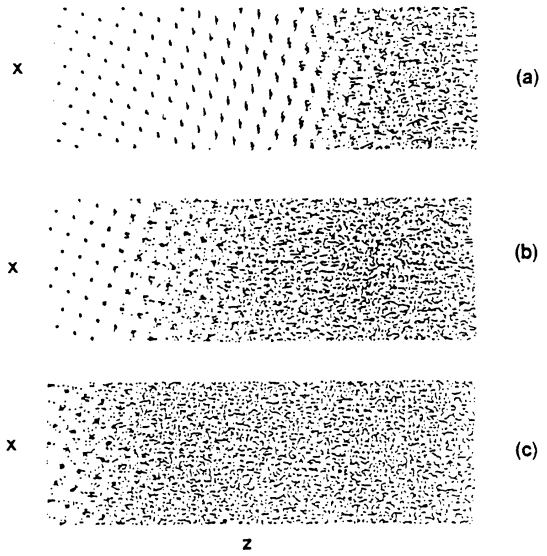

FIG. 6. Propagation of the disordered region, represented by the trajectory plot of accumulated atomic positions, each averaged over 1000 time steps (2.12 ps), in cell B at 875 K. Accumulation, each for a period of 20 000 time steps (42.4 ps), started at time steps (a) 50 000, (b) 70 000, and (c) 90 000. The model surface is to the right and the bulk material is to the left.

a faster rate of initial growth.

From the slope of the curves in Fig. 4 we obtain the propagation velocity of the disordered region at temperatures above 875 K. The results are shown in Fig. 5. A straight-line fit through these values gives a temperature of 865 ± 15 K, where the velocity vanishes. We will regard this value to be the thermodynamic melting temperature T_m of our interatomic potential model of aluminum. We note that the experiment value of T_m is 930 K. While the difference between model and experiment is of interest from the standpoint of judging the reality of the potential function, for purposes of studying thermal disordering and melting in the present model the relevant T_m is that determined for the model.

C. Surface behavior above T_m

We will examine the structural and kinetic behavior of cell B at 875 K. The purpose of this discussion will be to show that the disordered layers, characterized thus far only on the basis of $S(K)$, have the atomic structure, potential energy, and atomic mobility expected of a liquid layer, and therefore we are justified in interpreting Fig. 4 as showing the growth of a liquid region nucleated at the surface. The identification of the various characteristics of a liquidlike layer is also useful in later considerations of the surface behavior at temperatures below T_m.

We have seen in Fig. 4 that at 875 K, the significant behavior is the propagation of the melt-crystal interface. As the disordered (melt) region evolves in time, the potential energy of this region is found to have the same value as the liquid branch in Fig. 2. Figure 6 shows the advancement of the interface at three intervals during the simulation. Only a relatively small portion of the entire simulation cell, the part that contains the interface, is shown.

We have found that the radial distribution function $g(r)$ can be useful for distinguishing whether a layer is solid or liquid. In Figs. 7(a) and 7(b) we compare the $g(r)$ calculated for two adjacent layers identified as being disordered and ordered, respectively. These results are obtained using instantaneous atomic positions in Eq. (4). Figure 7(b) shows structural features characteristic of crystalline order, however, the appreciable broadening due to thermal motions makes such identifications less than definitive. In Figs. 7(c) and 7(d) we show results for the same layers, this time obtained using time-averaged atomic positions and considerably longer accumulation time. Comparing these results with those in Figs. 7(a) and 7(b), one sees that while $g(r)$ for the disordered layer is essentially unchanged, there is a pronounced difference for the ordered layer. The crystalline features of $g(r)$ shown in Fig. 7(d) are now unmistakable. The $g(r)$ in Figs. 7(a) and 7(c) have the same appearance as the radial distribution of a typical simple liquid. Comparing Figs. 7(c) and 7(d), one can conclude that the disappearance of the second-nearest-neighbor peak in $g(r)$ is a signature of the loss of the crystalline order. Our results also make it clear that in considering structural order at high temperatures, serious smearing effects are expected due to thermal vibrations of the atoms. By using time-averaged atomic positions, we have demonstrated that these effects can be essentially eliminated, making it possible to determine whether a layer in the simulation cell has a crystalline or liquidlike structure.

Another characteristic difference between solid and liquid is atomic mobility. In the present context we are concerned with direction-dependent atomic mobility in a given layer, a property which can be expressed through the mean-squared displacement (MSD) defined in Eq. (6). As expected, the temporal evolution of MSD can indicate whether the local environment in the layer has the characteristic of a solid or a liquid,[2,3] although such interpretations must take into account the microscopic nature of the spatial and time scales of the observation. We

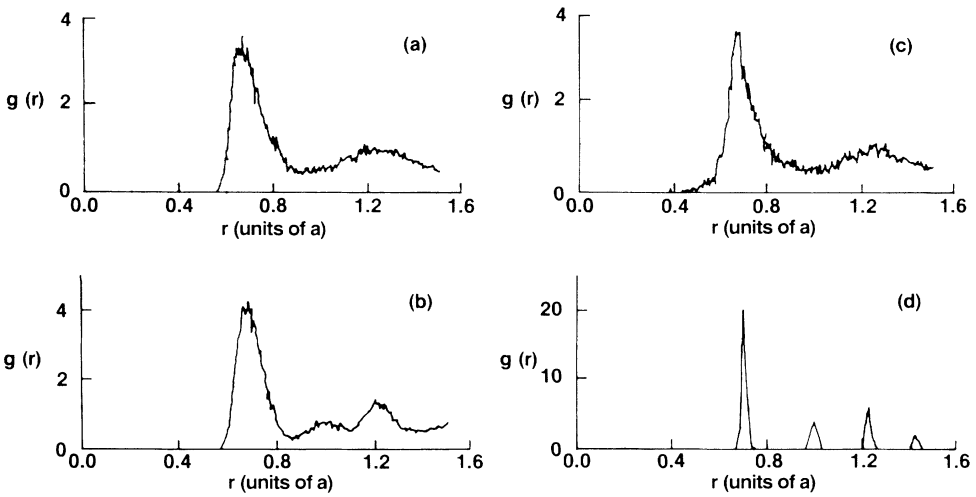

FIG. 7. Radial distribution functions $g(r)$ calculated for two adjacent layers in cell B at 875 K, one disordered (a) and (c) and the other ordered (b) and (d). Results are obtained using instantaneous atomic positions accumulated over 1000 time steps at 10-step intervals starting at time step 50 000 (a) and (b), or using atomic positions averaged over 1000 time steps accumulated over 50 000 time steps at 1000-step intervals starting at time step 50 000 (c) and (d).

have examined the results of MSD obtained using separately the x and y components of the atomic displacements and the z components. In a given layer, an onset of liquidlike mobility, manifested as a steady increase of MSD with time, was found to correlate with the onset of local melting. Therefore, as the melt-crystal interface propagated toward the bulk crystal, successive layers showed the onset of liquidlike mobility at successively later time, with the MSD curves showing essentially the same growth rate. For the liquidlike layers, an effective diffusion coefficient can be estimated from the average growth rate, MSD/t. We obtained a value of $(4.4\pm0.6)\times10^{-5}$ cm^2/s. This magnitude was also obtained in a direct calculation of the diffusion coefficient of liquid aluminum using a completely different potential function, in this case a pseudopotential.[23]

D. Surface behavior below T_m

In the region of high temperatures below T_m, the bulk layers may undergo structural disordering, but the process must be distinct from melting. When the system has a free surface, it is an open question whether surface-induced disordering can lead to local melting. We have initially studied cell B at 850 K. However, this turned out to be too close to T_m and it was difficult to obtain stable results. Therefore, a detailed study was carried out at 825 K.

We first consider layer profiles of potential energy and static structure factors time-averaged over certain durations at various stages during the simulation. These profiles showed that the layer of high energy is closely correlated with the layer showing structural disorder. As mentioned previously, metastable behavior was observed in the surface layers in the sense of a layer becoming disordered for some duration and then becoming ordered. Detailed examination of the outermost layers at the two free surfaces after simulation for 45 000 time steps, a significant period for local relaxation, shows the surfaces behaving independently; the right surface was well ordered, while the first few layers of the left surface appeared to be highly disordered. There seemed to be an intermediate region, between the disordered surface and the ordered substrate, where the atomic positions became

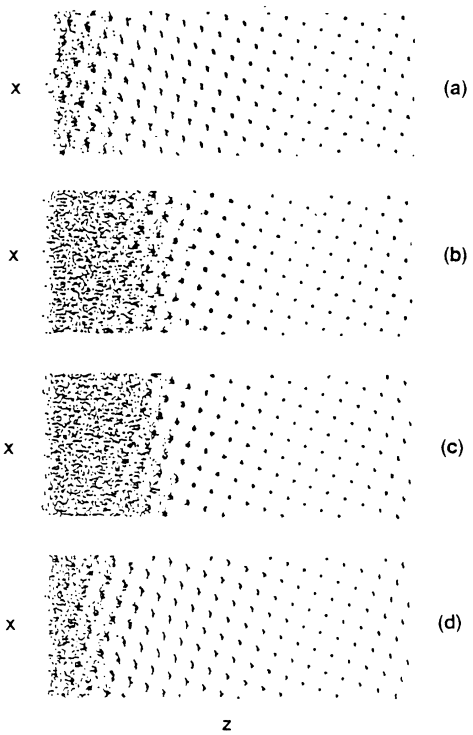

FIG. 8. Fluctuation of the surface-disordered region, represented by the trajectory plot of accumulated atomic positions, each averaged over 1000 time steps, in a surface region in cell B at 825 K (left side). Accumulation, each over a period of 20 000 time steps, started at time steps (a) 25 000, (b) 45 000, (c) 62 000, and (d) 98 000.

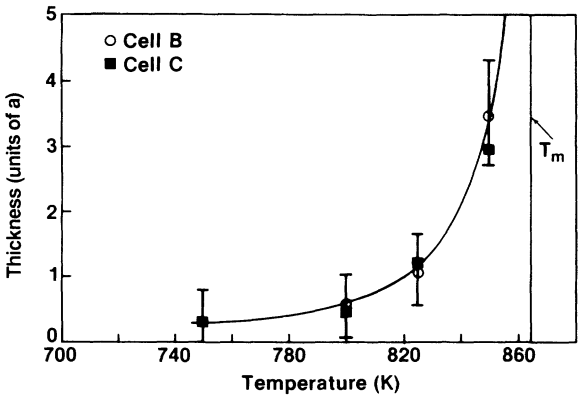

FIG. 9. Variation of thickness of disordered-surface region with temperature. Results for cell B and C are denoted by open circles and closed squares, respectively.

irregular and yet a faint remnant of the crystalline order of the substrate was still discernible. Figure 8(a)–8(d) show the time-averaged atomic positions in the left-surface region accumulated over a rather long time interval. The underlying structure of the substrate was clearly present at first [Fig. 8(a)], seemed to disappear during the middle portions of the simulation [Figs. 8(b) and 8(c)], and later re-emerged [Fig. 8(d)]. Thus the disordering of the region was only a metastable behavior as the system regained its memory of the substrate. These results indicate the need for long simulation intervals, since without such data one could be misled to conclude that the surface region has melted.

The re-emergence of structural order also has been observed in the radial distribution function. During the time interval when the layer was disordered, the behavior of $g(r)$ was liquidlike, but over a later time interval $g(r)$ for the same layer showed crystalline order. This suggests that during the interval of disordering, the atomic mobility should increase significantly, as was found to be the case when we examined the MSD results.

Our examination of thermal disordering at temperatures below T_m has shown that a structurally-disordered surface region exists which has a correspondingly higher potential energy and greater atomic mobility. Because the system temperature is below that of thermodynamic melting, one may regard this disordered region as that of a supercooled liquid. It is then of interest to characterize the spatial extent of the region, and follow its behavior as T_m is approached. Since the layers in the surface region can become intermittently disordered and ordered, the thickness of the disordered surface can be estimated only in a time-averaged sense, with the two surfaces treated independently as well. The results, shown in Fig. 9, indicate a gradual initial increase followed by a steep rise as the temperature approaches T_m. The limited data could be readily fitted to a $\ln(T_m - T)$ or a power law $(T - T_m)^n$ variation.

V. THERMAL DISORDERING IN A BICRYSTAL MODEL

Having examined how the free surfaces of a single crystal (cell B) behave over a range of temperatures above and below T_m, we are now in a position to study the disordering at a grain boundary (cell C) in a parallel fashion. The simulation runs carried out on the bicrystal model are summarized in Table III. While we have obtained data at the same temperatures as before, the focus of our discussion will be concerned with temperatures 800, 825, and 850 K. Notice that much longer runs were made at 825 and 850 K.

To see whether the bicrystal simulation cell conforms to our expectations of thermal and mechanical equilibrium, we have calculated at 825 K two layers of profiles of time-averaged temperature, pressure, and components of the stress tensor, one being an average over 2.1 ps and the other an average over 42 ps. From these results we conclude that across the cell the fluctuations in temperature are about 15 and 5%, respectively, for the two averages. In contrast, the pressure and stress components can be considered practically uniform in the sense of the long-time average, but on the basis of the short-time average there are sizable fluctuations in the layer profile. These data should be kept in mind as we consider the simulation results of our bicrystal model.

A. Surface behavior

Since cell C has both a grain boundary as well as two free surfaces, it is reasonable to ask whether these interfaces seriously affect each other because of finite system size. One way to demonstrate that the interfaces behave independently is to show that the free surfaces of cell C behave in the same manner as those of the reference system, cell B.

We have found that in the low-temperature range, 400–750 K, the surface structures are similar in both cells; they are well ordered during the entire simulation at these temperatures.

In the temperature range above T_m, 875–925 K, the liquid region at the surfaces grows steadily in cell C just as observed in cell B. There is agreement in the physical properties pertaining to potential energy, atomic struc-

TABLE III. Summary of simulation runs using the bicrystal model with free surfaces (Cell C) (Ref. 10). Results shown are the temperature T (K), number of time steps N_t, duration of simulation $N_t\Delta t$ (ps), pressure P (eV/a_0^3), potential energy per atom (eV/atom) in the bulk region and the grain-boundary region, U_b and U_{gb}, respectively. a_0 is the room-temperature lattice constant (4.05 Å). Standard deviation is given in parentheses, e.g., 3.525(5) means 3.525±0.005.

T	Nt	$N_t\Delta t$	P	U_b	U_{gb}
400	10 000	20.84	−0.030(20)	−3.525	−3.458(5)
500	10 000	20.91	−0.015(30)	−3.510	−3.422(5)
600	10 000	20.98	−0.033(30)	−3.493	−3.426(5)
700	10 000	21.05	−0.021(20)	−3.476	−3.407(5)
750	25 000	52.73	−0.025(30)	−3.467	−3.397(5)
800	37 000	78.20	−0.023(30)	−3.457	−3.387(7)
825	158 000	334.3	−0.021(40)	−3.453	−3.380(10)
850	223 000	472.4	−0.025(70)	−3.448	−3.370(10)
875	42 000	89.08	−0.026(30)	−3.442	−3.365(10)
900	23 000	48.84	−0.025(20)	−3.435	−3.360(10)
925	20 000	42.52	−0.020(30)	−3.425	−3.350(10)

ture, and atomic mobility of surface-nucleated liquid regions in the two systems. We have also repeated the determination of the propagation velocity of the crystal-melt interface and obtained the same value of T_m by extrapolation. Thus the presence of the *gb* interface appears not to affect the free-surface behavior at temperatures above T_m.

In the temperature range just below T_m, 800–850 K, the disordered region at the surface of the bicrystal model shows metastable behavior as expected from the above discussions of cell B. To complete the check of internal consistency, we find the time-averaged thickness of the disordered surface region is the same as before. Thus we conclude that the surface behavior is essentially the same in cells C and B.

B. Grain-boundary behavior

Given the detailed study of the free surface, it is natural to analyze the grain-boundary region in much the same way. Since the grain boundary may be regarded as an independent interface, it can be expected to act as a nucleation site for the onset of thermodynamic melting. We therefore analyze the grain-boundary (GB) region for evidence of local melting and to determine the propagation velocity of the melt-crystal interface. We find that within the error bars previously stated, the grain-boundary data lead to the same value of T_m (see Fig. 5). In the disordered regions which grow steadily in time, the energy, structure, and mobility behave like those of a liquid.

Since the temperature 850 K is too close to T_m, we again choose to examine in detail the behavior of the GB region at 825 K. Figure 10 shows the layer profiles of the potential energy and static structure factor, obtained in a similar way as in Fig. 2. At the cell center there is a narrow region with high layer energy closely correlated with the region of low $S(K)$. These properties define the core region of the grain boundary. More specifically, we will take the value of the potential-energy profile at the full width at half maximum to be the grain-boundary energy. The grain-boundary thickness is defined by the full width at half maximum of the $S(K)$ profile. Notice that in Fig. 10 the profiles are not stationary in time; this means that the grain boundary is able to migrate during the simulation.

Once we have defined the grain-boundary energy and thickness, we can follow their time variations as the system evolves. At 825 K, both quantities appear to undergo gradual changes, with higher energy correlated with larger thickness. Moreover, by examining the corresponding profiles of $S(K)$, we have found that, in general, the atomic configuration of the grain boundary is disordered if the thickness is less than two layers. Figure 11 shows the atomic trajectories extending over 500 steps at steps 60 000 and 90 000. These particular intervals are chosen to illustrate the very different atomic configurations in the grain-boundary region. As for atomic mobility, the bulk atoms are observed to be well localized at all times, while the atoms in the grain-boundary region can be quite mobile. We have found

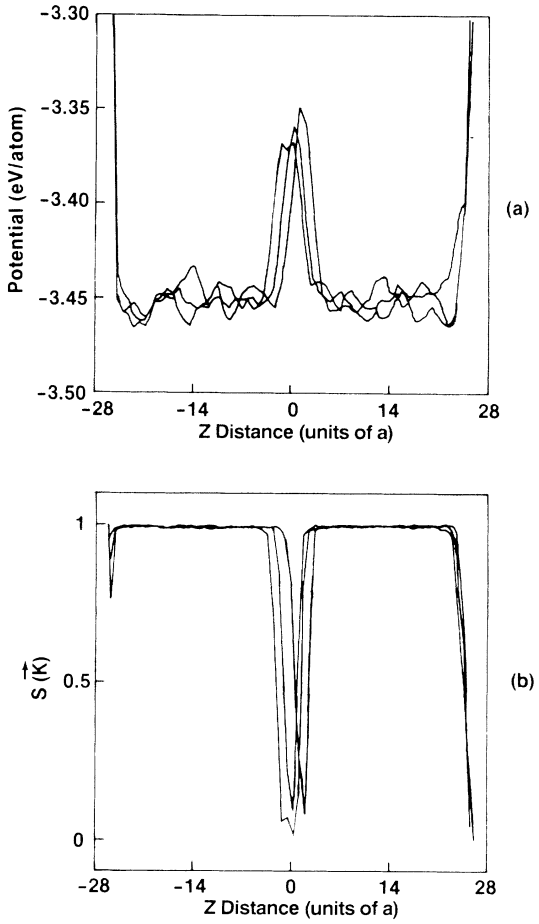

FIG. 10. Layer profiles of (a) potential energy and (b) static structure factor (time averaged over 1000 steps) for cell C at 825 K. Results shown are for three different times: steps 30 000, 60 000, and 90 000.

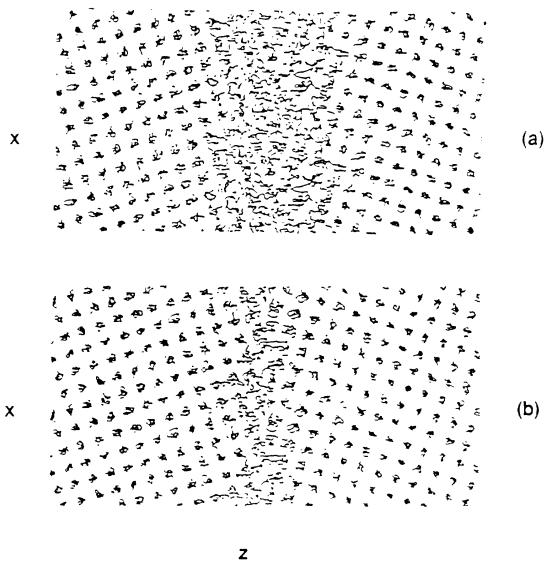

FIG. 11. Trajectory plot showing structural disorder at the grain-boundary interface in cell C at 825 K. Atomic positions are connected over 500 time steps at steps (a) 60 000 and (b) 90 000 during the simulation.

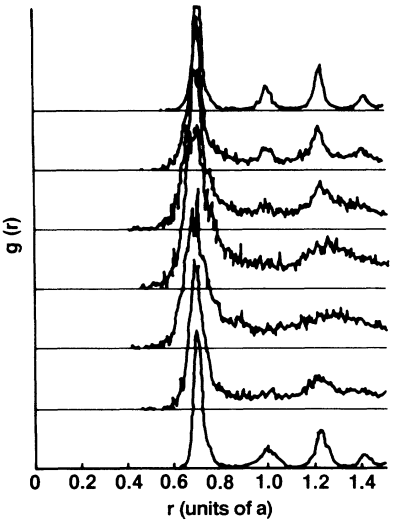

FIG. 12. Radial distribution function $g(r)$ for seven layers across the grain-boundary region in cell C at 825 K, showing the contrast between ordered bulk crystal layers and relatively disordered grain-boundary layers.

that some of the movements of the grain boundary involve a process of coupled sliding and migration.

Figure 12 shows the time-averaged $g(r)$, averaged over 1000 steps and accumulated over 20 000 steps, at step 60 000 for different regions across the grain-boundary core at 825 K. Based on these distributions one can distinguish the disordered core region from the ordered bulk. Later, at step 90 000 the distributions show a much more ordered core. This kind of metastability is similar to that discussed in Sec. IV at 825 K.

Finally, it is interesting to note that the average potential energy of the grain-boundary core falls on a curve that merges rather smoothly with the liquid-state branch at T_m, as shown in Fig. 13 (also compare with Fig. 3).

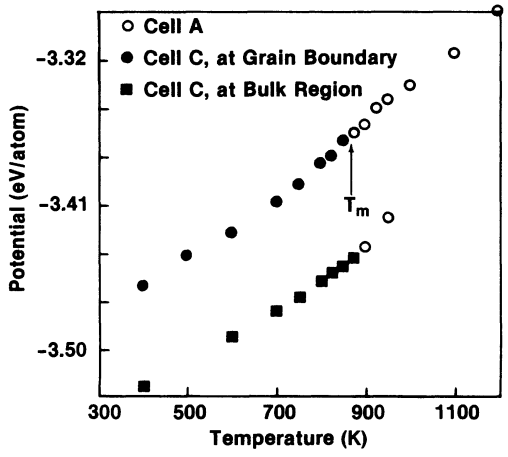

FIG. 13. Variation of potential energy per atom in the grain-boundary region using cell C (closed circles). Also shown are potential energy values for single-crystal cell A (open circles) and for bulk region of cell C (closed squares).

VI. SUMMARY AND CONCLUSION

In this work we have investigated the effects of an interface (free surface or grain boundary) on atomic disordering and local melting by molecular-dynamics simulation using a series of three models: a single crystal in bulk environment; a single crystal with free surfaces; and a bicrystal with free surfaces. By systematically studying the local structure, potential energy, and atomic mobility in each model over a temperature range from below to above the bulk melting point, we have shown that the different physical properties calculated layerwise from the simulation data give a consistent picture of the character of atomic disordering. This consistency extends to the behavior of the bulk and surface regions from one model to another.

Several aspects of the present simulation make the results more plausible than previous molecular-dynamics studies. First, the interatomic potential function adopted for the simulation, constructed by the embedded-atom method, is believed to be more realistic for fcc metals than the early empirical potentials, most of which have only two adjustable parameters compared to six for the EAM construction. Aside from the better theoretical justification for the EAM potential, the fact that it is fitted to the elastic constants, sublimation energy, lattice constant, and vacancy formation energy means that a reasonable description of the cohesive energy, stress relaxation, surface behavior, and atomic mobility can be expected. A second improvement is our use of the same free-surface border condition for the single-crystal and bicrystal cells. Atomic disordering behavior on free surfaces is of intrinsic interest by itself. From the standpoint of studying internal interfaces, this condition is preferable to the periodic border condition which unavoidably introduces a second grain boundary, and to the fixed border condition with its undesirable constraining effects. Furthermore, the method we used to determine T_m makes the use of free-surface border condition for the bicrystal cell a natural choice. Another factor contributing to reliable results is the considerably longer simulation runs made at certain temperatures. These data demonstrate the metastable behavior that characterizes disordering at $T < T_m$.

Assuming that the bulk melting point T_m of our simulation model has been properly determined by extrapolation of surface-nucleated melting velocity, the grain-boundary interface modeled here does not lose its crystalline order at all the temperatures studied below T_m. This finding is based on the detailed study of disordering in the grain-boundary region below T_m, and is also supported by the extrapolation of grain-boundary-nucleated melting velocity above T_m. Our conclusion concerning grain-boundary premelting effects is in agreement with existing simulations[2,11,12] and with TEM experiments.[9] It is, however, different from that reached in our own previous work.[3] This difference can be traced to the incorrect identification of T_m made in the earlier work. As we have shown by the results described in Secs. III and IV, the melting transition observed in a single-crystal model with periodic border conditions occurs at a temperature

greater than T_m.

An aspect of our work that appears not to have been addressed in previous simulation studies is the nature of disordering in the free-surface or grain-boundary region at temperatures just below T_m. We believe our results on the energy-temperature variation (see Fig. 3 and discussion) and the re-emergence of structural order after a long run (see Fig. 8 and discussion) are evidence suggesting the onset of metastable behavior, and, along with the growth of interfacial thickness as one approaches T_m (Fig. 9), it is tempting to regard such data as possibly supporting the theoretical prediction that thermal disordering on a crystal surface is a continuous process, in contrast to the first-order melting transition in the bulk.[20] On the other hand, one should keep in mind that on the short time and distance scales of molecular-dynamics simulation, kinetic-barrier effects could mask any "intrinsic metastability behavior" in the sense of local energy minima. Since the former are expected to be sensitive to system sizes, some assessment of their presence can be made by using larger simulation cells. To explicitly demonstrate metastability, one could examine the potential-energy surfaces obtained by applying energy minimization to a sufficient number of system configurations generated during the molecular-dynamics simulation.[24] The concept of inherent structure,[23] extended to an inhomogeneous system such as an interface, may well be relevant to the understanding of competing effects between ordering in the bulk and disordering at the interface.

ACKNOWLEDGMENTS

We are grateful to S. M. Foiles for constructing the EAM potential used in this study. We are also indebted to D. Wolf, J. Lutsko, and S. R. Phillpot for invaluable discussions and for showing us the method of melting-point determination used here. T.N. and S. Y. thank Argonne National Laboratory for partial support during the course of this work. T. N. also acknowledges partial support by the U.S. Department of Energy and the encouragement provided by R. Craig Williamson. The computations reported in this work were performed at the IBM Thomas J. Watson Research Center.

---

*Present address: IBM East Fishkill, Hopewell Junction, NY 12533.

†Present address: Center for Materials Science and Engineering, University of Texas, Austin, TX 78712.

[1]H. Gleiter and B. Chalmers, *High-Angle Grain Boundaries* (Pergamon, Oxford, 1972).

[2]G. Ciccotti, M. Guillope, and V. Pontikis, Phys. Rev. B **27**, 5576 (1983); M. Guillope, G. Ciccotti, and V. Pontikis, Surf. Sci. **144**, 67 (1984).

[3]T. Nguyen, P. S. Ho, T. Kwok, C. Nitta, and S. Yip, Phys. Rev. Lett. **57**, 1919 (1986); P. S. Ho, T. Kwok, T. Nguyen, C. Nitta, and S. Yip, Scr. Metall. **19**, 993 (1985).

[4]P. Deymier, A. Taiwo, and G. Kalonji, Acta Metall. **35**, 2719 (1987).

[5]J. Q. Broughton and G. H. Gilmer, Phys. Rev. Lett. **56**, 2692 (1986).

[6]V. Pontikis, J. Phys. **49**, (Paris) Colloq. C5-327 (1988).

[7]K. T. Aust, Can. Metall. Q **8**, 173 (1969); P. Lagarde and M. Biscondi, Can. Metall. Q **13**, 245 (1974); D. W. Demianczuk and K. T. Aust, Acta Metall. **23**, 1149 (1975).

[8]T. Watanabe, S. I. Kimura, and S. Karashima, Philos. Mag. A **49**, 845 (1984).

[9]T. E. Hsieh and R. W. Balluffi, Acta Metall. **37**, 1637 (1989).

[10]T. Nguyen, Ph.D. thesis, MIT, 1988.

[11]S. R. Phillpot, J. F. Lutsko, D. Wolf, and S. Yip, Phys. Rev. B **40**, 2831 (1989).

[12]J. F. Lutsko, D. Wolf, S. R. Phillpot, and S. Yip, Phys. Rev. B **40**, 2841 (1989).

[13]J. F. Lutsko, D. Wolf, S. Yip, S. R. Phillpot, and T. Nguyen, Phys. Rev. B **38**, 11 752 (1988).

[14]D. Wolf, J. Phys. (Paris) Colloq. **46**, C4-197 (1985); D. Wolf and J. F. Lutsko, Z. Kristallogr. Kristallgeom. Kristallphys. Kristalllchem. **189**, 239 (1989).

[15]M. J. Weins, H. Gleiter, and B. Chalmers, J. Appl. Phys. **42**, 2639 (1971); M. Hashimoto, Y. Ishida, R. Yammamoto, and M. Doyama, J. Phys. **10**, 1109 (1980); see also Ref. 2.

[16]M. S. Daw and M. I. Baskes, Phys. Rev. B **29**, 6443 (1984); S. M. Foiles, M. I. Baskes, and M. S. Daw, *ibid.* **79**, 83 (1985). The particular potential used in this study was supplied to us by S. M. Foiles.

[17]E. Clementi and C. Roetti, At. Data Nucl. Data Tables **14**, 177 (1974).

[18]J. H. Rose, J. R. Smith, F. Guinea, and J. Ferrante, Phys. Rev. B **29**, 2963 (1984).

[19]J. M. W. Frenken, P. M. J. Maree, and J. F. van der Veen, Phys. Rev. B **34**, 7506 (1986).

[20]R. Lipowsky, Phys. Rev. Lett. **49**, 1575 (1982); R. Lipowsky and W. Speth, Phys. Rev. B **28**, 3983 (1983).

[21]F. H. Stillinger and T. A. Weber, Phys. Rev. B **31**, 5262 (1985).

[22]J. Q. Broughton and X. P. Li, Phys. Rev. B **35**, 9120 (1987).

[23]I. Ebbsjo, T. Kinell, and I. Waller, J. Phys. C **13**, 1865 (1980).

[24]F. H. Stillinger and T. A. Weber, J. Chem. Phys. **80**, 4434 (1984).